
FAST AND AUTOMATIC FULL WAVEFORM INVERSION BY DUAL AUGMENTED LAGRANGIAN

Kamal Aghazade

Institute of Geophysics, Polish Academy of Sciences, Warsaw, Poland.
aghasade.kamal@igf.edu.pl

Ali Gholami

Institute of Geophysics, Polish Academy of Sciences, Warsaw, Poland,
agholami@igf.edu.pl

December 13, 2024

ABSTRACT

Full Waveform Inversion (FWI) stands as a nonlinear, high-resolution technology for subsurface imaging via surface-recorded data. This paper introduces an augmented Lagrangian dual formulation for FWI, rooted in the viewpoint that Lagrange multipliers serve as fundamental unknowns for the accurate linearization of the FWI problem. Once these multipliers are estimated, the determination of model parameters becomes simple. Therefore, unlike traditional primal algorithms, the proposed dual method circumvents direct engagement with model parameters or wavefields, instead tackling the estimation of Lagrange multipliers through a gradient ascent iteration. This approach yields two significant advantages: i) the background model remains fixed, requiring only one LU matrix factorization for each frequency inversion. ii) Convergence of the algorithm can be improved by leveraging techniques like quasi-Newton I-BFGS methods and Anderson acceleration. Numerical examples from elastic and acoustic FWI utilizing different benchmark models are provided, showing that the dual algorithm converges quickly and requires fewer computations than the standard primal algorithm.

1 Introduction

Full waveform inversion (FWI) is a widely used seismic imaging technique with a focus on reconstruction of the physical properties of the subsurface (e.g., velocity, density, attenuation, conductivity, permittivity, and anisotropic parameters) [1, 2]. It has a broad application in various field of geoscience such as global seismology (see e.g., [3], and references therein), ground penetration radar (GPR) [4, 5], CO₂ characterization [6], glaciology [7], near surface studies by inversion of surface waves [8], geothermal studies [9], and volcanology [10].

Even though FWI can be performed in either the time or frequency domain, this paper focuses on frequency domain FWI [11].

1.1 Forward Problem

1.1.1 Acoustic media

For a given medium characterized by the model parameters vector $\mathbf{m} \in \mathbb{R}^{n \times 1}$ (squared slowness), the data vector $\mathbf{d} \in \mathbb{C}^{n_r \times 1}$ is calculated by first solving the Helmholtz equation

$$(\omega^2 \text{diag}(\mathbf{m}) + \Delta)\mathbf{u} = \mathbf{b}, \quad (1)$$

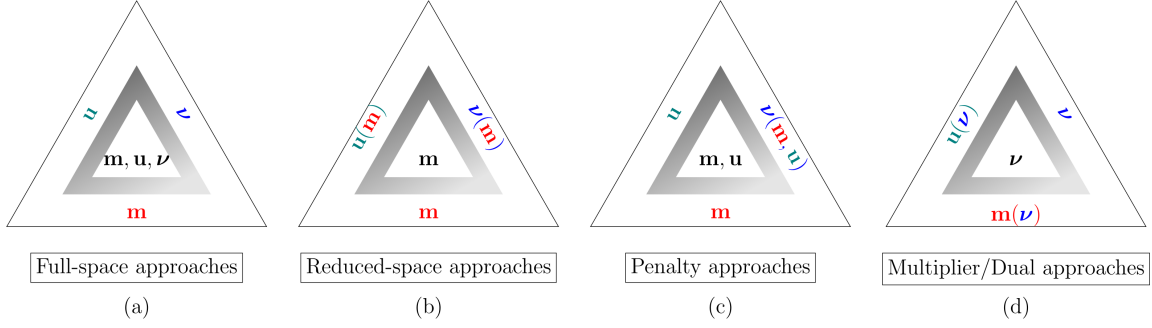


Figure 1: Different FWI formulations: (a) Full-space approach, which treats \mathbf{m} , \mathbf{u} , and $\boldsymbol{\nu}$ as optimization parameters; (b) Conventional FWI formulation, which eliminates the wavefield and Lagrange multipliers from the optimization variables; (c) Penalty formulation, which eliminates only the Lagrange multipliers from the optimization variables; (d) The approach proposed in this study, which eliminates the model parameters and wavefield from the optimization variables.

for the wavefield $\mathbf{u} \in \mathbb{C}^{n \times 1}$. The monochromatic wavefield \mathbf{u} is then sampled at the receiver locations using the sampling operator $\mathbf{P} \in \mathbb{R}^{n_r \times n}$, i.e., $\mathbf{d} = \mathbf{P}\mathbf{u}$. In these equations, ω denotes angular frequency, Δ is Laplace operator, $\mathbf{b} \in \mathbb{C}^{n \times 1}$ is the source term, n is the number of model parameters, and n_r denotes the number of receivers.

Equation (1) can be discretized following the methodology described in [12]. The discretized equation can be written in matrix-vector form as $\mathbf{A}(\mathbf{m})\mathbf{u} = \mathbf{b}$. Here, $\mathbf{A}(\mathbf{m}) = (\omega^2 \text{diag}(\mathbf{m}) + \Delta) \in \mathbb{C}^{n \times n}$ represents the Helmholtz operator, which is constructed with sufficient accuracy and suitable boundary conditions. Following the bi-linearity of the wave equation, it is also possible to write (1) as $\mathbf{L}(\mathbf{u})\mathbf{m} = \mathbf{y}(\mathbf{u})$, where $\mathbf{L}(\mathbf{u}) = \omega^2 \text{diag}(\mathbf{u})$, and $\mathbf{y}(\mathbf{u}) = \mathbf{b} - \Delta\mathbf{u}$.

1.1.2 Elastic media

The elastic wave equation can be defined as:

$$\begin{aligned} \rho\omega^2\mathbf{u}_x + (\lambda + 2\mu)\partial_{xx}\mathbf{u}_x + \mu\partial_{zz}\mathbf{u}_x + (\lambda + \mu)\partial_{xz}\mathbf{u}_z &= \mathbf{b}_x \\ (\lambda + \mu)\partial_{xz}\mathbf{u}_x + \rho\omega^2\mathbf{u}_z + (\lambda + 2\mu)\partial_{zz}\mathbf{u}_z + \mu\partial_{xx}\mathbf{u}_z &= \mathbf{b}_z \end{aligned} \quad (2)$$

where $\rho \in \mathbb{R}^{n \times 1}$ is mass density, $\lambda \in \mathbb{R}^{n \times 1}$ and $\mu \in \mathbb{R}^{n \times 1}$ denote Lamé parameters, $\mathbf{u}_x \in \mathbb{C}^{n \times 1}$ and $\mathbf{u}_z \in \mathbb{C}^{n \times 1}$ are horizontal and vertical particle displacements, and $\mathbf{b}_x \in \mathbb{C}^{n \times 1}$, $\mathbf{b}_z \in \mathbb{C}^{n \times 1}$ are the source terms. Using the definition of P- and S- wave velocities:

$$V_P = \sqrt{\frac{\lambda + 2\mu}{\rho}}, \quad V_S = \sqrt{\frac{\mu}{\rho}},$$

and assuming a constant density medium, then (2) can be discretized and written in matrix-vector form as $\mathbf{A}(\mathbf{m})\mathbf{u} = \mathbf{b}$ where

$$\mathbf{m} = \begin{pmatrix} \mathbf{m}_P := V_P^2 \\ \mathbf{m}_S := V_S^2 \end{pmatrix}, \quad \mathbf{u} = \begin{pmatrix} \mathbf{u}_x \\ \mathbf{u}_z \end{pmatrix}, \quad \mathbf{b} = \begin{pmatrix} \mathbf{b}_x \\ \mathbf{b}_z \end{pmatrix}. \quad (3)$$

In this case, $\mathbf{A}(\mathbf{m}) \in \mathbb{C}^{2n \times 2n}$ is the elastic forward operator, $\mathbf{u} \in \mathbb{C}^{2n \times 1}$ and $\mathbf{b} \in \mathbb{C}^{2n \times 1}$ includes the vertical and horizontal components of the wavefield and source, respectively. Also, $\mathbf{d} = \mathbf{P}\mathbf{u} \in \mathbb{C}^{2n_r \times 1}$ is the recorded data and $\mathbf{P} \in \mathbb{R}^{2n_r \times 2n}$ is the sampling operator. The employed squared velocity parameterization also allows writing (2) as $\mathbf{L}(\mathbf{u})\mathbf{m} = \mathbf{y}(\mathbf{u})$, where $\mathbf{L}(\mathbf{u}) = \frac{\partial \mathbf{A}(\mathbf{m})}{\partial \mathbf{m}}\mathbf{u}$ is defined as

$$\mathbf{L}(\mathbf{u}) = \begin{bmatrix} \text{diag}(\partial_{xx}\mathbf{u}_x + \partial_{xz}\mathbf{u}_z) & \text{diag}(\partial_{zz}\mathbf{u}_x - \partial_{xz}\mathbf{u}_z) \\ \text{diag}(\partial_{zz}\mathbf{u}_z + \partial_{xz}\mathbf{u}_x) & \text{diag}(\partial_{xx}\mathbf{u}_z - \partial_{xz}\mathbf{u}_x) \end{bmatrix},$$

and $\mathbf{y}(\mathbf{u}) = \mathbf{b} - \omega^2\mathbf{u}$.

1.2 Inverse Problem

Mathematically, for the given source term \mathbf{b} and the observed data \mathbf{d} , the inverse problem is to estimate the model parameters \mathbf{m} . This can be defined as a non-linearly constrained optimization problem, thorough which a data misfit

term is minimized while simultaneously the wave equation is satisfied [13]:

$$\underset{\mathbf{m}, \mathbf{u}}{\text{minimize}} \quad \frac{1}{2} \|\mathbf{P}\mathbf{u} - \mathbf{d}\|_2^2 \quad \text{subject to} \quad \mathbf{A}(\mathbf{m})\mathbf{u} = \mathbf{b}. \quad (4)$$

The well-established method of Lagrange multipliers can be used to solve the inverse problem [14]. This approach involves optimization of the Lagrangian function, defined as

$$\mathcal{L}(\mathbf{m}, \mathbf{u}, \boldsymbol{\nu}) = \frac{1}{2} \|\mathbf{P}\mathbf{u} - \mathbf{d}\|_2^2 + \boldsymbol{\nu}^T (\mathbf{A}(\mathbf{m})\mathbf{u} - \mathbf{b}), \quad (5)$$

where $\boldsymbol{\nu}$ is the dual variable (or Lagrange multipliers associated to the wave-equation constraints). \mathbf{x}^T denote the complex conjugate transpose of vector \mathbf{x} . The optimum point of the Lagrangian is a saddle-point which attains a minimum over the primal variables \mathbf{m} and \mathbf{u} and a maximum over the dual variable $\boldsymbol{\nu}$. Different approaches have been proposed to solve the problem and find the optimum point (see Fig. 1).

1.2.1 Full-space approaches

In the so-called full-space approach, the optimization is performed simultaneously over the variables \mathbf{m} , \mathbf{u} , and $\boldsymbol{\nu}$ (Fig. 1a). Two strategies can be adopted for this approach. The first is the so-called all-at-once method, where the optimization is conducted jointly over all three variables [15]. This is typically achieved using a Newton-Krylov method, which solves the associated optimality conditions. Alternatively, a sequential optimization strategy can be employed, where the Lagrangian or augmented Lagrangian (AL) is optimized with respect to one of the variables \mathbf{m} , \mathbf{u} , and $\boldsymbol{\nu}$ at a time, while the other two variables are held constant [16–18].

1.2.2 Reduced-space approaches

To address the memory complexity associated with handling all variables, a second group of methods eliminates the wavefield and multipliers from the set of optimization variables through variable projection [19], thereby satisfying the wave equation constraint exactly. This approach expresses the wavefield and multipliers as implicit functions of \mathbf{m} , i.e., $\mathbf{u}(\mathbf{m})$, $\boldsymbol{\nu}(\mathbf{m})$ (Fig. 1b), leading to a more complicated objective function that depends only on the model parameters. As a result, the dimensionality of the search space is reduced. However, the reduced objective function is highly sensitive to the initial model and is challenging to optimize due to ill-conditioning and difficulties in tuning the step length [1]. Considerable effort has been made to improve the reduced FWI (e.g., [20–25]).

1.2.3 Penalty approaches

One approach to address the ill-conditioning issue of the reduced FWI is to include a damping term in the Lagrangian, which penalizes the Lagrange multipliers. This method allows us to compute the Lagrange multipliers as a closed-form function of the model parameters and the wavefield, denoted as $\boldsymbol{\nu}(\mathbf{m}, \mathbf{u})$. Consequently, this enables their elimination from the optimization variables, resulting in the quadratic penalty formulation of the FWI [26]. The penalty approach in FWI requires optimization of the penalty function over \mathbf{m} and \mathbf{u} (Fig. 1c). This optimization can be performed through an alternating optimization method known as wavefield reconstruction inversion (WRI) [26]. Additionally, it is possible to further eliminate the associated wavefields to construct a more complex reduced penalty objective function, which is then optimized solely over \mathbf{m} [27]. For a comprehensive review of penalty-based FWI, see [18]. However, the implementation of WRI suffers from inaccurate estimation of the Lagrange multipliers, which can significantly reduce the performance of the method, particularly when the initial model is erroneous [28].

A more advanced FWI algorithm can be achieved through the proximal regularization of the Lagrangian [29], which regularizes the Lagrange multipliers by keeping them close to their previous estimates rather than damping them to zero, as done in penalty-based methods [28]. This approach is equivalent to the standard AL-based FWI [16]. In this method, optimization is performed over all three classes of parameters: \mathbf{m} , \mathbf{u} , and $\boldsymbol{\nu}$ (Fig. 1a). The proximal regularization employed by the AL method significantly enhances the performance of the FWI algorithm, particularly shown on synthetic data [16, 30].

1.3 Contributions

In this paper, we develop, for the first time, a dual approach for FWI, where the model parameters and wavefield are expressed as implicit functions of the Lagrange multipliers, $\mathbf{m}(\boldsymbol{\nu})$ and $\mathbf{u}(\boldsymbol{\nu})$ (Fig. 1d). This formulation allows us to eliminate \mathbf{m} and \mathbf{u} from the optimization variables, leading to a dual AL function dependent solely on $\boldsymbol{\nu}$. The proposed dual approach reduces the FWI problem to the estimation of accurate Lagrange multipliers by solving the dual objective function. Once the multipliers are estimated, the FWI problem can be resolved efficiently in a single iteration.

The dual function is maximized using a gradient ascent algorithm, which can be further accelerated by applying the limited memory BFGS (l-BFGS) [31] or Anderson Acceleration (AA) techniques [32, 33]. A main advantage of this dual formulation is that for each frequency, the associated multiplier is estimated based on the initial model for that frequency. Consequently, the wave equation operator is dependent on the initial model and remains fixed during the iteration. Therefore, only a single lower-upper triangular (LU) decomposition is necessary to invert each data frequency, akin to the standard contrast source inversion method [34]. However, while the standard contrast source inversion is based on the penalty formulation of FWI, the proposed algorithm utilizes the AL formulation. Thus, it combines the computational efficiency of contrast source inversion with the accuracy of the AL algorithm.

The proposed algorithm is tested using both acoustic and elastic data. The results demonstrate that accurate results can be obtained efficiently and fully automatically.

Section 2 presents the theory behind the dual AL method. In Section 3, the algorithm for implementing the dual AL method is detailed, including aspects such as acceleration techniques, parameter selection, and computational complexity. Section 4 provides a comparison of the dual algorithm with traditional methods like FWI and WRI. Finally, Section 5 shows numerical experiments using both acoustic and elastic data.

2 FWI by Dual AL method

The AL for the problem (4) is defined as

$$\mathcal{L}_\mu(\mathbf{m}, \mathbf{u}, \boldsymbol{\nu}) = \mathcal{L}(\mathbf{m}, \mathbf{u}, \boldsymbol{\nu}) + \frac{\mu}{2} \|\mathbf{A}(\mathbf{m})\mathbf{u} - \mathbf{b}\|_2^2, \quad (6)$$

where \mathcal{L} is the standard Lagrangian defined in (5) and $\mu > 0$ is the penalty parameter. Optimization of the AL function requires minimization of it with respect to the primal variables \mathbf{m} and \mathbf{u} and maximization over the Lagrange multiplier $\boldsymbol{\nu}$.

The dual problem is defined as

$$\max_{\boldsymbol{\nu}} \mathcal{D}_\mu(\boldsymbol{\nu}), \quad (7)$$

where

$$\mathcal{D}_\mu(\boldsymbol{\nu}) = \min_{\mathbf{m}, \mathbf{u}} \mathcal{L}_\mu(\mathbf{m}, \mathbf{u}, \boldsymbol{\nu}). \quad (8)$$

It can be shown that the gradient of the dual function has the following simple form (see [35]):

$$\frac{\partial}{\partial \boldsymbol{\nu}} \mathcal{D}_\mu(\boldsymbol{\nu}) = \mathbf{A}(\mathbf{m}(\boldsymbol{\nu}))\mathbf{u}(\boldsymbol{\nu}) - \mathbf{b}, \quad (9)$$

where $\mathbf{m}(\boldsymbol{\nu})$ and $\mathbf{u}(\boldsymbol{\nu})$ are the model parameters and the wavefield that are obtained by minimizing the AL function for a given multiplier vector $\boldsymbol{\nu}$.

2.1 Computation of $\mathbf{m}(\boldsymbol{\nu})$ and $\mathbf{u}(\boldsymbol{\nu})$

The $\mathbf{m}(\boldsymbol{\nu})$ and $\mathbf{u}(\boldsymbol{\nu})$ are defined as

$$\arg \min_{\mathbf{m}, \mathbf{u}} \mathcal{L}_\mu(\mathbf{m}, \mathbf{u}, \boldsymbol{\nu}). \quad (10)$$

It may not be possible to find closed-form expressions for $\mathbf{m}(\boldsymbol{\nu})$ and $\mathbf{u}(\boldsymbol{\nu})$ that minimize \mathcal{L}_μ in terms of $\boldsymbol{\nu}$. However, good approximations can be obtained in the neighborhood of an initial model \mathbf{m}_0 . For a given initial model \mathbf{m}_0 , the wavefield $\mathbf{u}(\boldsymbol{\nu})$ minimizing \mathcal{L}_μ satisfies

$$(\mathbf{P}^T \mathbf{P} + \mu \mathbf{A}_0^T \mathbf{A}_0) \mathbf{u}(\boldsymbol{\nu}) = \mathbf{P}^T \mathbf{d} + \mu \mathbf{A}_0^T \mathbf{b} - \mathbf{A}_0^T \boldsymbol{\nu}. \quad (11)$$

where $\mathbf{A}_0 \equiv \mathbf{A}(\mathbf{m}_0)$. It can be shown that the wavefield also satisfies [28]

$$\mathbf{A}_0 \mathbf{u}(\boldsymbol{\nu}) = \mathbf{b} + \boldsymbol{\lambda}(\boldsymbol{\nu}) - \frac{1}{\mu} \boldsymbol{\nu}, \quad (12)$$

where

$$\boldsymbol{\lambda}(\boldsymbol{\nu}) = \mathbf{S}_0^T (\mathbf{S}_0 \mathbf{S}_0^T + \mu \mathbf{I})^{-1} (\delta \mathbf{d}_0 + \frac{1}{\mu} \mathbf{S}_0 \boldsymbol{\nu}), \quad (13)$$

with $\mathbf{S}_0 = \mathbf{P} \mathbf{A}_0^{-1}$ and $\delta \mathbf{d}_0 = \mathbf{d} - \mathbf{S}_0 \mathbf{b}$.

Regarding the minimizer $\mathbf{m}(\boldsymbol{\nu})$, partial derivative of \mathcal{L}_μ with respect to \mathbf{m} is

$$\frac{\partial \mathcal{L}_\mu}{\partial \mathbf{m}} = \hat{\mathbf{L}}(\boldsymbol{\nu})^T \boldsymbol{\nu} + \mu \hat{\mathbf{L}}(\boldsymbol{\nu})^T [\hat{\mathbf{L}}(\boldsymbol{\nu}) \mathbf{m}(\boldsymbol{\nu}) - \hat{\mathbf{y}}(\boldsymbol{\nu})]. \quad (14)$$

where $\hat{\mathbf{L}}(\boldsymbol{\nu}) \equiv \mathbf{L}(\mathbf{u}(\boldsymbol{\nu}))$ and $\hat{\mathbf{y}}(\boldsymbol{\nu}) \equiv \mathbf{y}(\mathbf{u}(\boldsymbol{\nu}))$ (see Section 1.1 for the definition of \mathbf{L} and \mathbf{y}). Using (12) and the equality

$$\hat{\mathbf{L}}(\boldsymbol{\nu}) \mathbf{m}_0 - \hat{\mathbf{y}}(\boldsymbol{\nu}) = \mathbf{A}_0 \mathbf{u}(\boldsymbol{\nu}) - \mathbf{b},$$

and letting $\frac{\partial \mathcal{L}_\mu}{\partial \mathbf{m}} = 0$, we get

$$\mathbf{m}(\boldsymbol{\nu}) = \mathbf{m}_0 - [\hat{\mathbf{L}}(\boldsymbol{\nu})^T \hat{\mathbf{L}}(\boldsymbol{\nu})]^{-1} \hat{\mathbf{L}}(\boldsymbol{\nu})^T \boldsymbol{\lambda}(\boldsymbol{\nu}). \quad (15)$$

3 Algorithm Description

The dual algorithm presented above is closely related to standard AL algorithms for FWI [16–18, 28], with one key difference: in the dual algorithm, the background model remains fixed, and the focus shifts to estimating the associated multiplier. In this case, the stiffness matrix depends solely on the background medium, which remains unchanged throughout the inversion process. Consequently, when using a direct solver, such as the LU decomposition method, the finite-difference (FD) operator is factorized and the Hessian matrix is computed only once. These results can then be reused for multiple sources and across successive iterations of the inversion [34].

Using a scaled Lagrange multiplier $\boldsymbol{\varepsilon} = \frac{1}{\mu} \boldsymbol{\nu}$, the forward/backward wavefields $\mathbf{u}(\boldsymbol{\varepsilon})/\boldsymbol{\lambda}(\boldsymbol{\varepsilon})$ can be computed using either of the following approaches [28]:

1. Wavefield-oriented approach:

$$\mathbf{u}(\boldsymbol{\varepsilon}) = (\mathbf{P}^T \mathbf{P} + \mu \mathbf{A}_0^T \mathbf{A}_0)^{-1} (\mathbf{P}^T \mathbf{d} + \mu \mathbf{A}_0^T (\mathbf{b} - \boldsymbol{\varepsilon})), \quad (16)$$

$$\boldsymbol{\lambda}(\boldsymbol{\varepsilon}) = \boldsymbol{\varepsilon} + \mathbf{A}_0 \mathbf{u}(\boldsymbol{\varepsilon}) - \mathbf{b}. \quad (17)$$

2. Multiplier-oriented approach:

$$\boldsymbol{\lambda}(\boldsymbol{\varepsilon}) = \mathbf{S}_0^T (\mathbf{S}_0 \mathbf{S}_0^T + \mu \mathbf{I})^{-1} (\delta \mathbf{d}_0 + \mathbf{S}_0 \boldsymbol{\varepsilon}), \quad (18)$$

$$\mathbf{u}(\boldsymbol{\varepsilon}) = \mathbf{A}_0^{-1} (\mathbf{b} + \boldsymbol{\lambda}(\boldsymbol{\varepsilon}) - \boldsymbol{\varepsilon}). \quad (19)$$

Then the gradient of the dual objective is simply $\mathbf{g}(\boldsymbol{\varepsilon}) = \mathbf{A}(\mathbf{m}(\boldsymbol{\varepsilon})) \mathbf{u}(\boldsymbol{\varepsilon}) - \mathbf{b}$, which allows us to solve the problem by the standard gradient based algorithms [14]. The steepest ascent method is the simplest algorithm for maximizing the dual objective function, as it only requires computing the gradient of the objective function at each iteration. Algorithms 1 and 2 summarize respectively the multiplier-oriented and wavefield-oriented forms of the dual method for multi-frequency FWI. Due to the high computational cost of computing the forward and backward wavefields at each iteration of the optimization, improving the algorithm's convergence rate can be of great significance. In the following, we describe two acceleration methods that require only the gradient to be supplied.

3.1 Quasi-Newton l-BFGS method

The update direction provided by the Newton's method is

$$\mathbf{x}_k = \mathbf{H}_k^{-1} \mathbf{g}_k, \quad (20)$$

where k is the iteration number, \mathbf{g}_k is the gradient at iteration k , and \mathbf{H}_k is the Hessian matrix of the dual function at iteration k . Computing the inverse of the Hessian at each iteration can be challenging. A quasi-Newton method iteratively approximates the Hessian matrix, with the l-BFGS method being one of the most popular. l-BFGS updates the Hessian approximation using changes in both the solution and the gradient at each iteration [14]:

$$\mathbf{H}_{k+1} = \mathbf{H}_k + \frac{\delta \mathbf{g}_k \delta \mathbf{g}_k^T}{\delta \mathbf{g}_k^T \delta \boldsymbol{\varepsilon}_k} - \frac{\mathbf{H}_k \delta \boldsymbol{\varepsilon}_k \delta \boldsymbol{\varepsilon}_k^T \mathbf{H}_k^T}{\delta \boldsymbol{\varepsilon}_k^T \mathbf{H}_k \delta \mathbf{g}_k}, \quad (21)$$

where $\delta \boldsymbol{\varepsilon}_k = \boldsymbol{\varepsilon}_{k+1} - \boldsymbol{\varepsilon}_k$ and $\delta \mathbf{g}_k = \mathbf{g}_{k+1} - \mathbf{g}_k$. Having computed the update direction \mathbf{x}_k , the multiplier is updated as

$$\boldsymbol{\varepsilon}_{k+1} = \boldsymbol{\varepsilon}_k + \alpha_k \mathbf{x}_k, \quad (22)$$

where α_k is the step length and is chosen to satisfy the Wolfe conditions. Despite relying solely on the gradient, l-BFGS provides a sufficiently accurate approximation of the objective function to achieve superlinear convergence.

3.2 Anderson acceleration

The gradient ascent algorithm for updating the multiplier may be defined as a fixed-point iteration:

$$\varepsilon_{k+1} = g(\varepsilon_k) := \varepsilon_k + \mathbf{A}(\mathbf{m}(\varepsilon_k))\mathbf{u}(\varepsilon_k) - \mathbf{b}. \quad (23)$$

This enables the use of acceleration strategies to improve convergence rates, such as Anderson Acceleration (AA) [32]. In this paper, we employ AA. For a detailed implementation of AA in solving (23), the reader is referred to [33]. In [33], the AA method was applied to improve the convergence of the wavefield-oriented AL approach in acoustic FWI, where the search space includes not only the Lagrange multipliers but also the model parameters and the wavefield.

Algorithm 1 Multiplier-oriented dual AL algorithm for FWI.

Require: Observed data \mathbf{d} , source \mathbf{b} , initial model \mathbf{m} , fixed data tolerance δ_ω

- 1: **for** $\omega \in [\omega_{min}, \omega_{max}]$ **do**
 - 2: Compute LU factorization of the Helmholtz operator $\mathbf{A}_0 = \mathbf{A}(\mathbf{m})$ at the frequency ω
 - 3: Form the data-space Hessian matrix $\mathbf{Q} = \mathbf{S}_0 \mathbf{S}_0^T = \mathbf{P} \mathbf{A}_0^{-1} \mathbf{A}_0^{-T} \mathbf{P}^T$
 - 4: Set $\varepsilon_0 = \mathbf{0}$
 - 5: **for** $k = 1, 2, \dots, maxit$ **do**
 - 6: $\delta \mathbf{d}_\omega = \mathbf{d}_\omega - \mathbf{S}_0(\mathbf{b}_\omega - \varepsilon_{k-1})$
 - 7: Solve $\|(\frac{1}{\mu} \mathbf{Q} + \mathbf{I})^{-1} \delta \mathbf{d}_\omega\|_2 = \delta_\omega$ for μ
 - 8: $\boldsymbol{\lambda} = \mathbf{S}_0^T (\mathbf{Q} + \mu \mathbf{I})^{-1} \delta \mathbf{d}_\omega$
 - 9: $\mathbf{u} = \mathbf{A}_0^{-1} (\mathbf{b}_\omega + \boldsymbol{\lambda} - \varepsilon_{k-1})$
 - 10: $\delta \mathbf{m} = (\mathbf{L}(\mathbf{u})^T \mathbf{L}(\mathbf{u}))^{-1} \mathbf{L}(\mathbf{u})^T \boldsymbol{\lambda}$
 - 11: $\varepsilon_k = \varepsilon_{k-1} + \mathbf{A}(\mathbf{m} + \delta \mathbf{m})\mathbf{u} - \mathbf{b}_\omega$
 - 12: **end for**
 - 13: Use $\delta \mathbf{m}$ obtained at the current frequency to update the model, $\mathbf{m} \leftarrow \mathbf{m} + \delta \mathbf{m}$, and use it for the inversion at the next higher frequency.
 - 14: **end for**
-

Algorithm 2 Wavefield-oriented dual AL algorithm for FWI.

Require: Observed data \mathbf{d} , source \mathbf{b} , initial model \mathbf{m} , fixed data tolerance δ_ω , initial μ

- 1: **for** $\omega \in [\omega_{min}, \omega_{max}]$ **do**
 - 2: Build $\mathbf{A}_0 = \mathbf{A}(\mathbf{m})$ at the frequency ω and compute LU factorization of the augmented Helmholtz operator $(\mathbf{P}^T \mathbf{P} + \mu \mathbf{A}_0^T \mathbf{A}_0) = \hat{\mathbf{L}} \hat{\mathbf{U}}$
 - 3: Set $\varepsilon = \mathbf{0}$
 - 4: **for** $k = 1, 2, \dots, maxit$ **do**
 - 5: $\mathbf{u} = \hat{\mathbf{U}}^{-1} \hat{\mathbf{L}}^{-1} (\mathbf{P}^T \mathbf{d}_\omega + \mu \mathbf{A}_0^T (\mathbf{b}_\omega - \varepsilon_{k-1}))$
 - 6: $\boldsymbol{\lambda} = \varepsilon_{k-1} + \mathbf{A}_0 \mathbf{u} - \mathbf{b}_\omega$
 - 7: $\delta \mathbf{m} = (\mathbf{L}(\mathbf{u})^T \mathbf{L}(\mathbf{u}))^{-1} \mathbf{L}(\mathbf{u})^T \boldsymbol{\lambda}$
 - 8: $\varepsilon_k = \varepsilon_{k-1} + \mathbf{A}(\mathbf{m} + \delta \mathbf{m})\mathbf{u} - \mathbf{b}_\omega$
 - 9: **end for**
 - 10: $\mu = (\|\mathbf{P} \mathbf{u} - \mathbf{d}_\omega\|_2 + \delta_\omega) / (2 \|\mathbf{P} \mathbf{u} - \mathbf{d}_\omega\|_2) \mu$
 - 11: Use $\delta \mathbf{m}$ obtained at the current frequency to update the model, $\mathbf{m} \leftarrow \mathbf{m} + \delta \mathbf{m}$, and use it for the inversion at the next higher frequency.
 - 12: **end for**
-

3.3 On penalty parameter selection

Accurate determination of the penalty parameter μ is crucial for avoiding the ill-conditioning of the problem and to fit the data at the desired level. At each iteration of the algorithm, the discrepancy principle strategy is employed to automatically determine this parameter, which requires solving the following 1D-root finding problem [28]:

$$\phi(\mu) := \|(\frac{1}{\mu} \mathbf{Q} + \mathbf{I})^{-1} \delta \mathbf{d}\|_2 = \delta_\omega, \quad (24)$$

(line 7 of Algorithm 1) where δ_ω is an estimate of the norm of noise of data at frequency ω . In this case, the Lagrange multiplier fits the scattered data with the specified noise level. The determination of μ in the multiplier-oriented

algorithm (Algorithm 1) is handled efficiently, even for large-scale problems, as the matrix $\mathbf{Q} = \mathbf{S}_0 \mathbf{S}_0^T$ is sized according to the number of receivers and is computed prior to the iteration. This precomputation allows for careful tuning of μ at each iteration. However, in the wavefield-oriented approach, the parameter μ defines the augmented operator $(\mathbf{P}^T \mathbf{P} + \mu \mathbf{A}_0^T \mathbf{A}_0)$, which is of the size of the model, making it more difficult to adjust μ at each iteration. For this reason, Algorithm 2 employs a fixed value of μ for each frequency. The value of μ is determined in line 10 of Algorithm 2 based on the method proposed in [36].

3.4 Computational Complexity

The dual AL method, as presented in Algorithms 1 and 2, introduces an efficient alternative strategy that retains the advantages of the original primal/dual AL method while addressing its computational limitations.

3.4.1 Algorithm 1

The computational complexity for LU factorization of \mathbf{A}_0 is $O(n^3)$, while each forward/backward substitution has a complexity of $O(n^2)$. After computing the LU factorization of \mathbf{A}_0 , the matrix \mathbf{Q} requires $2n_r$ forward/backward substitutions, leading to a total cost of $O(2n_r \times n^2)$ floating-point operations.

Assuming the inversion of \mathbf{Q} is negligible, the complexity for lines 6, 8, and 9 is dominated by $O(2n_s \times n^2)$. Therefore, the overall complexity of Algorithm 1 is driven by the $O(n^3)$ factor, and for n_ω frequencies, the total complexity becomes $O(n_\omega \times n^3)$.

3.4.2 Algorithm 2

In this case, the LU factorization of $(\mathbf{P}^T \mathbf{P} + \mu \mathbf{A}_0^T \mathbf{A}_0)$ (line 3) has a complexity of $O(n^3)$. At each inner iteration, the wavefield is computed with a complexity of $O(2n_s \times n^2)$ (line 6). Given that these are the dominant operations, for n_ω frequencies, the total complexity is also $O(n_\omega \times n^3)$.

Thus, both Algorithms 1 and 2 have a computational complexity of $O(n_\omega \times n^3)$. However, since Algorithm 1 allows for more efficient fine-tuning of the penalty parameter μ , it is used for the numerical examples in this paper. Furthermore, Algorithm 1 is suitable for the time-domain.

In the standard AL algorithm, the background model is treated as an optimization variable that needs to be updated at each (inner) iteration [16]. For n_ω frequencies, this results in a total computational complexity of $O(\text{maxit} \times n_\omega \times n^3)$. Consequently, the speedup achieved by the proposed dual algorithm over the original primal-dual approach is approximately proportional to maxit , representing the number of inner iterations required to invert each frequency.

4 Interpretation of the Dual method

This section gives a brief description of the strategy which the dual algorithm may be interpreted.

Consider the acoustic FWI, which aims to simultaneously find the wavefield \mathbf{u} and the model \mathbf{m} that satisfy both the wave equation $\mathbf{A}(\mathbf{m})\mathbf{u} = \mathbf{b}$ and the data equation $\mathbf{P}\mathbf{u} = \mathbf{d}$. Due to the nonlinearity of the problem, iterative linearization is typically applied. Starting from an initial model \mathbf{m}_0 , the wave equation can be expressed as [28]:

$$\mathbf{A}_0 \mathbf{u} = \mathbf{b} - \omega^2 \text{diag}(\delta \mathbf{m}) \mathbf{u}_0 - \omega^2 \text{diag}(\delta \mathbf{m}) \delta \mathbf{u}, \quad (25)$$

where $\delta \mathbf{m} = \mathbf{m} - \mathbf{m}_0$, $\delta \mathbf{u} = \mathbf{u} - \mathbf{u}_0$, and \mathbf{u}_0 is a known incident wavefield.

The nonlinear term $-\omega^2 \text{diag}(\delta \mathbf{m}) \delta \mathbf{u}$ on the right-hand side accounts for higher-order scattering and is typically neglected to linearize the equation. In this case, if \mathbf{u}_0 satisfies $\mathbf{A}_0 \mathbf{u}_0 = \mathbf{b}$, the first-order Born approximation is achieved, which forms the basis of conventional FWI algorithms [1, 11]. It is also possible to obtain a more accurate incident wavefield that simultaneously satisfies $\mathbf{A}_0 \mathbf{u}_0 = \mathbf{b}$ and $\mathbf{P} \mathbf{u}_0 = \mathbf{d}$ in the least-squares sense, as employed in wavefield reconstruction inversion (WRI) [26]:

$$\begin{pmatrix} \beta \mathbf{A}_0 \\ \mathbf{P} \end{pmatrix} \mathbf{u}_0 = \begin{pmatrix} \beta \mathbf{b} \\ \mathbf{d} \end{pmatrix}, \quad (26)$$

where $\beta > 0$ is a balancing parameter. In this case, the approximation goes beyond the first-order Born approximation, resulting in a more accurate linearization [18]. In both cases, some higher-order scattering terms are neglected and are subsequently compensated for by updating the model parameters at each iteration.

In order to see how the dual algorithm works, let us substitute $\lambda(\epsilon)$ from (18) into (19), giving

$$\mathbf{A}_0 \mathbf{u}(\epsilon) = \mathbf{b} + \mathbf{p} + \mathbf{q}(\epsilon), \quad (27)$$

Table 1: Examples and associated acquisition parameters were utilized to gather data regarding the benchmark models.

| Example no. | Inversion type | Model name | Model dimension (km) | Grid size | Grid interval (m) | Source no. | Receiver no. |
|-------------|----------------|---------------------|----------------------|-------------------|-------------------|------------|--------------|
| I | Acoustic | Marmousi II | 3.5×17.1 | 281×1361 | 12.5 | 137 | 137 |
| II | Acoustic | 2004 BP | 12×67.5 | 160×900 | 75 | 450 | 67 |
| II | Elastic | SEG/EAGE overthrust | 4.67×20 | 187×801 | 25 | 134 | 400 |

where

$$\mathbf{p} = (\mathbf{S}_0^T \mathbf{S}_0 + \mu \mathbf{I})^{-1} \mathbf{S}_0^T \delta \mathbf{d}_0, \quad (28)$$

$$\mathbf{q}(\epsilon) = -\mu (\mathbf{S}_0^T \mathbf{S}_0 + \mu \mathbf{I})^{-1} \epsilon. \quad (29)$$

We observe that the first two terms on the right-hand side are fixed and independent of ϵ . It can be shown that \mathbf{p} corresponds exactly to the source extension used in the WRI method. The last term, $\mathbf{q}(\epsilon)$, is linearly dependent on ϵ and accounts for the higher-order scattering neglected in WRI.

Consequently, unlike traditional methods that compensate for higher-order scattering, the source of the problem's nonlinearity, by iteratively updating the model parameters, the dual algorithm focuses on directly estimating the nonlinear term while keeping the background model fixed. Once this nonlinear term is accurately estimated, the problem becomes fully linearized and can be solved in a single iteration.

5 Numerical Examples

This section evaluates the computational efficiency and accuracy of the proposed dual-AL method for constant-density (equal to unity) acoustic- and elastic-FWI in isotropic media. For all examples, the model error is computed as

$$\text{ME}(\%) = 100 \times \|\mathbf{m} - \mathbf{m}^*\|_2 / \|\mathbf{m}^*\|_2,$$

where \mathbf{m}^* denotes the true model.

5.1 Acoustic inversion

For acoustic media, the model parameterization is based on the squared slowness ($\mathbf{m} = \mathbf{V}_p^{-2}$). The Marmousi II and 2004 BP models are assessed for the purpose validating our inversion algorithm. The wave equation is discretized using a nine-point stencil finite-difference technique, which includes the incorporation of an antilumped mass. The stencil coefficients are adjusted based on frequency, as described in [12]. Furthermore, absorbing boundary conditions are implemented along all boundaries.

Throughout the examples, the inversion stage is carried out for specific frequencies within a set of inversion paths, using the established multiscale frequency continuation approach. In this method, the result of each path is used as the starting model for the subsequent path.

5.1.1 Example I: dual-AL versus AL

The first example focuses on comparing dual-AL and AL algorithms in terms of accuracy and computational efficiency using Marmousi II velocity model (Fig. 2a). The information regarding the dimension of the model, grid size, grid interval, number of sources and receivers are summarized in Table 1 (first row). Simulation is performed with a surface acquisition setup using the Ricker wavelet with a dominant frequency of 10 Hz as the source function. The inversion process for each method starts with a one-dimensional starting model that exhibits a linear increase from 1.5 km/s to 4.5 km/s. It subsequently takes two paths for inversion, in which frequency range covered by each path is from 3 Hz to 15 Hz, with intervals of 0.5 Hz.

The AL approach involves a total of 540 iterations. Within these iterations, frequencies of 3 Hz and 3.5 Hz are processed in 20 iterations, while the remaining frequencies undergo inversion in 10 iterations each. This task necessitates the computation of 540 LU factorizations. In contrast, the dual-AL technique requires performing 1 LU factorization per frequency, resulting in a total of 50 LU factorizations. The dual-AL method also includes the same number of iterations to update the dual variable.

The final inversion results achieved by the AL and dual-AL algorithms are presented in Fig. 2b and Fig. 2c, respectively. The dual-AL approach exhibits remarkable accuracy, despite the substantial redundancy in computational tasks and runtime associated with LU factorizations as summarized in Table. 2.

Table 2: Quantitative comparison of the dual-AL and AL methods for acoustic FWI of the Marmousi II model.

| Method | LU no. | Runtime (h) | ME (%) |
|---------|--------|-------------|--------|
| AL | 540 | 7.75 | 7.62 |
| dual-AL | 50 | 3.63 | 8.75 |

In order to highlight the importance of the dual update, the l-BFGS (with memory of 10) and AA techniques (with a history of 3) are employed. The reconstructed models of this evaluation are shown in Fig. 2d (for l-BFGS) and Fig. 2e (for AA), each one with an overall higher accuracy compared to the original dual-AL method. However, the accuracy of the dual-AL technique with AA was found to be superior than both original dual-AL and AL methods, as can be verified by the quantitative comparison in terms of computed model errors versus number of LU factorizations (Fig. 3). Moreover, a well-behaved convergence curve is observed in the case of dual-AL based experiments. Furthermore, the velocity models that have been reconstructed using the aforementioned methods are compared to the true model at various horizontal distances (Fig. 4). Based on this comparison, the dual-AL approach with AA outperforms the other methods in accurately capturing the deeper parts of the model. Hence, the AA approach is employed in the subsequent examples.

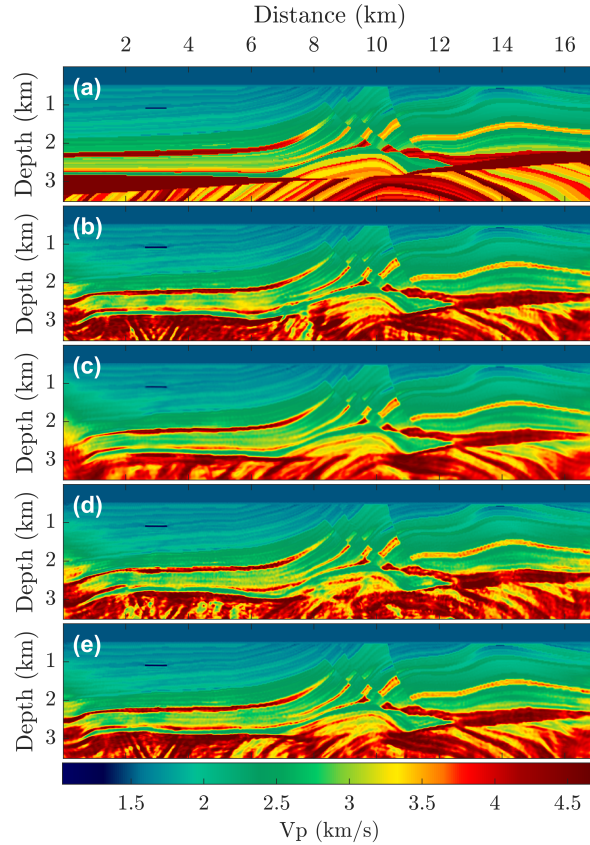


Figure 2: The Marmousi test. (a) True model, inversion results achieved by AL (b), dual-AL (c), dual-AL accelerated by l-BFGS with a memory of 10 (d), and dual-AL accelerated by AA with a history of 3 (e).

5.1.2 Example II: dual-AL against challenging 2004 BP salt model

The performance of the dual-AL algorithm is evaluated using the challenging 2004 BP salt model (Fig. 5a). The information regarding model and acquisition parameters are summarized in Table. 1 (second row). An ultra-long-offset stationary-recording acquisition is carried out, in which the pressure sources are 150 m apart at a depth of 25 m and the hydrophones are equally distributed 1 km apart on the seafloor. To enhance computation efficiency, the Green functions spatial reciprocity is utilized to treat sources as receivers and vice versa. The source signature is the Ricker

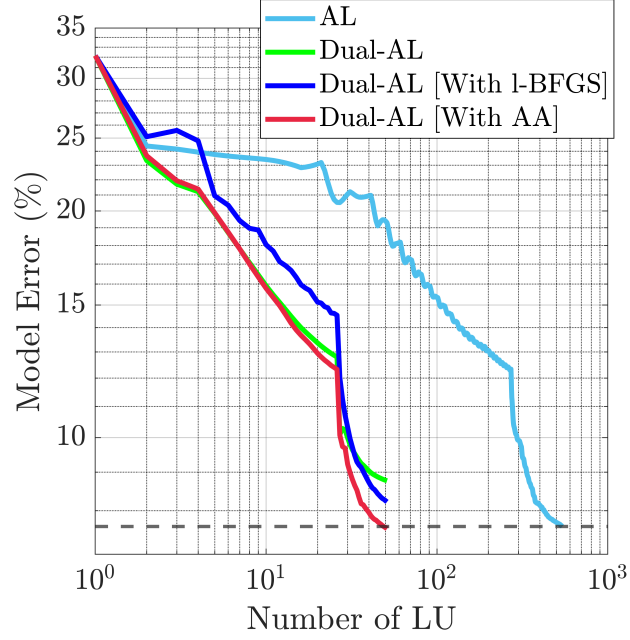


Figure 3: The Marmousi test. The evolution of the computed model error versus number of LU factorization for four different methods: AL, dual-AL, dual-AL by l-BFGS with a memory of 10, and dual-AL by AA with a history of 3.

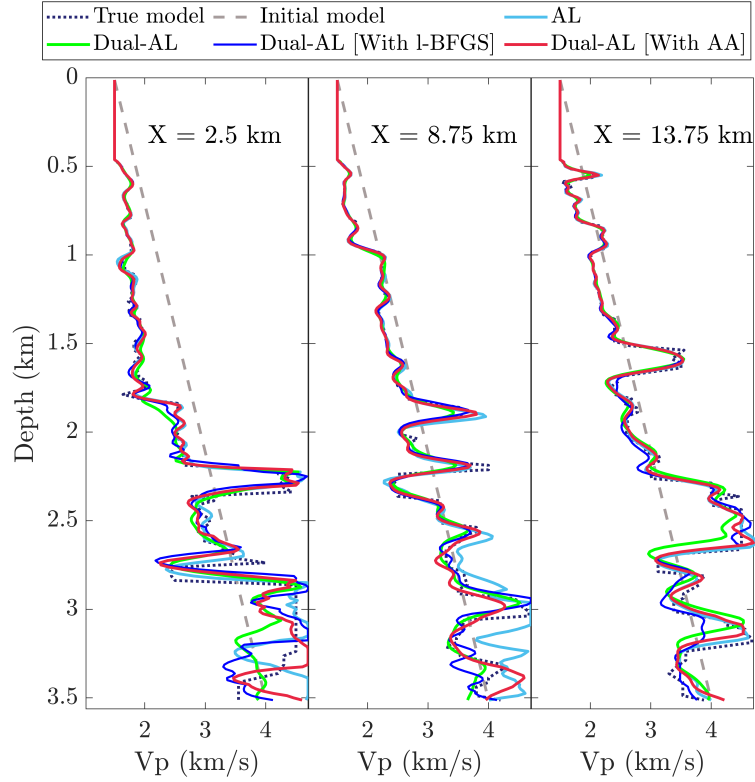


Figure 4: Comparison of the vertical velocity profiles extracted from true model, initial model, and the reconstructed models (Figure 2) at different horizontal distances labelled as $X = 2.5$ km, 8.75 km, and 13.75 km.

wavelet with a dominate frequency of 3 Hz. A one-dimensional initial model was utilized for the inversion (Fig. 5b),

starting at the data frequency of 1 Hz. According to [37], the above factors presents significant complexities that pose challenges for FWI methods because they often get stuck in a local minimum.

The inversion procedure consisted of four separate paths, each involving the inversion of frequencies within certain ranges. The ranges were 1 Hz to 2.5 Hz, 1 Hz to 3.0 Hz, 1 Hz to 3.5 Hz, and 1 Hz to 4.5 Hz, with a frequency gap of 0.5 Hz inside each. Individual frequency inversions were performed, each with 1 LU factorization and 10 inner iterations to update the dual variable, resulting in a total of 23 LU factorizations.

First, the algorithm is evaluated on a noise-free data set. The inversion result shown in Fig. 5c demonstrates the great accuracy of the proposed dual-AL approach, which can be further improved with regularization. Figure. 5d illustrates the use of total variation (TV) regularization for suppressing noise-like artifacts. The noise-contaminated data set is next subjected to a similar analysis. To achieve this, Gaussian random noise with a standard deviation equal to 15% of the mean absolute value of each monochromatic data set is added. Figures 5e and 5f illustrate the inversion results without and with TV regularization, respectively. Compared to noise-free data (Fig. 5c), the algorithm maintains resilience in the presence of noise (Fig. 5e) thanks to the automatic determination of the regularization parameter in (24). A quantitative comparison of the evolution of the model error over the number of LU factorizations is shown in Fig. 6, confirming the robustness of the proposed method in the presence of noise, as well as the efficacy of TV regularization in improving the results.

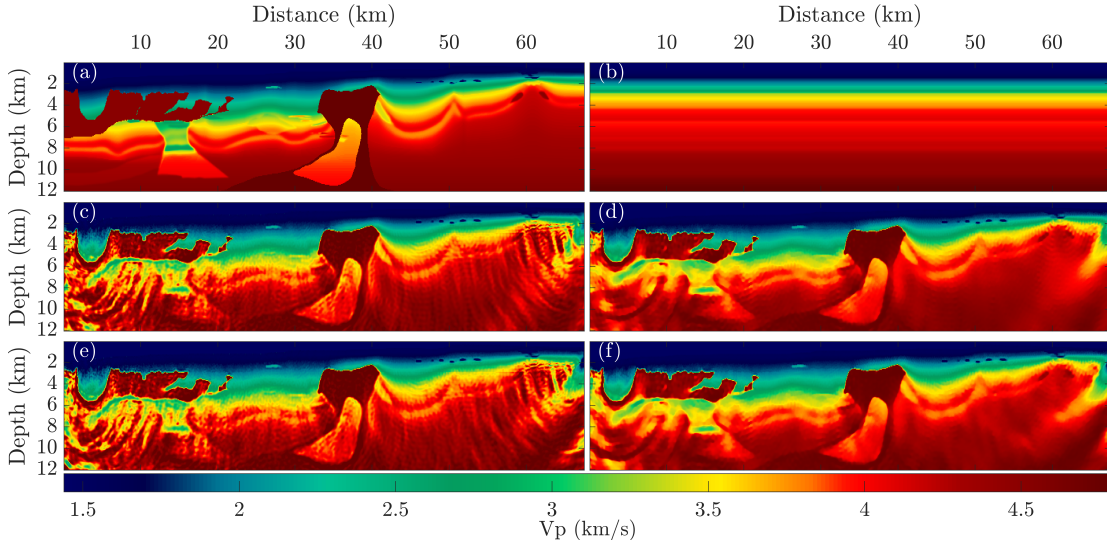


Figure 5: 2004 BP model example. (a) True model, and (b) initial model. The inversion results obtained by dual-AL algorithm for the noise-free scenario without regularisation (c) and with TV regularisation (d). (e-f) same as (c-d) for noise contaminated data.

5.2 Elastic inversion

For elastic media, the model parameterization is based the squared P- and S-wave velocities, $\mathbf{m} = (\mathbf{m}_P, \mathbf{m}_S) := (V_P^2, V_S^2)$, following [38]. A 2D section of the 3D SEG/EAGE overthrust is used and the benchmark model to test the proposed inversion algorithm. From this V_P model, the V_S model is derived using empirical relation proposed in [39], which makes the inversion more difficult because of the existence of various Poisson's ratios within the medium. Forward modeling engine is developed based on the method described in [40]. Furthermore, absorbing boundary conditions are implemented along all boundaries.

Throughout the examples, the inversion stage is carried out for specific frequencies within a set of inversion paths, using the established multiscale frequency continuation approach. In this method, the result of each path is used as the starting model for the subsequent path.

The V_P model and empirically derived V_S model are shown in Fig. 7a and Fig. 7b, respectively with the additional information summarized in Table. 1 (third row). The surface acquisition setup for the modeling consists of the Ricker wavelet sources (in horizontal and vertical directions) with dominant frequencies of 10 Hz at intervals of 150 m. The receivers are two-component sensors that are positioned at intervals of 50 m. The inversion stage initiated with the initial V_P and V_S models, respectively shown in Fig. 7c and Fig. 7d.

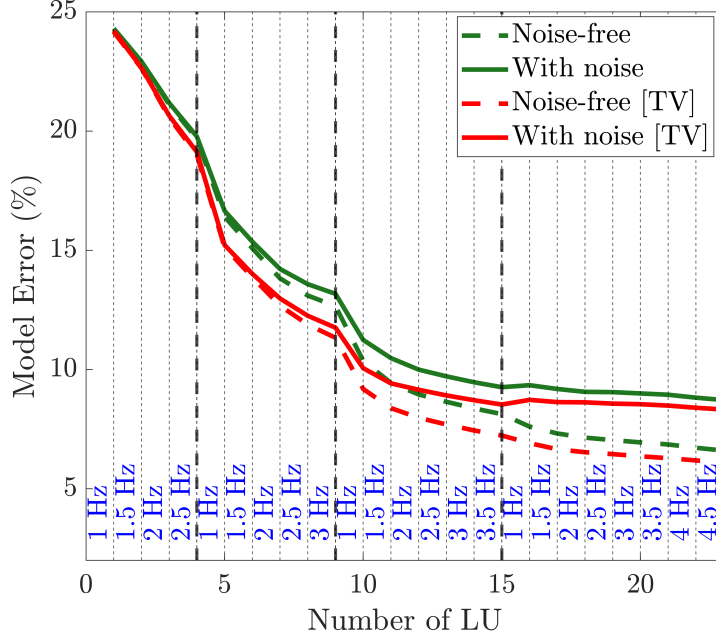


Figure 6: 2004 BP test. The evolution of the model error versus number of LU factorizations for the estimated models shown in Fig. 5.

The inversion process consists of three frequency bands: 3 Hz to 6 Hz, 3 Hz to 7.5 Hz, and 3 Hz to 13 Hz, with increments of 0.5 Hz. This results in a total of 38 mono-frequency inversions. Assuming 10 iterations per frequency, a total of 380 iterations were performed. The performance of the dual-AL algorithm is compared to the original AL method [38]. For this example, the AL method requires 380 LU factorizations (one LU factorization per iteration). In contrast, the dual-AL method requires only 38 LU factorizations, with 10 inner iterations per frequency to update the dual variable using AA with a history of 6. The inversion results are shown in Fig. 8. It can be seen that the reconstructed velocities obtained by the dual-AL method (Fig. 8c-d) are quite comparable to that of AL (Fig. 8a-b). This observation is verified by the difference plots (the difference between true and reconstructed velocity models) shown in Fig. 9. Overall, the dual-AL method, outperforms the AL approach, which can be verified by the computed model errors shown in Fig. 10.

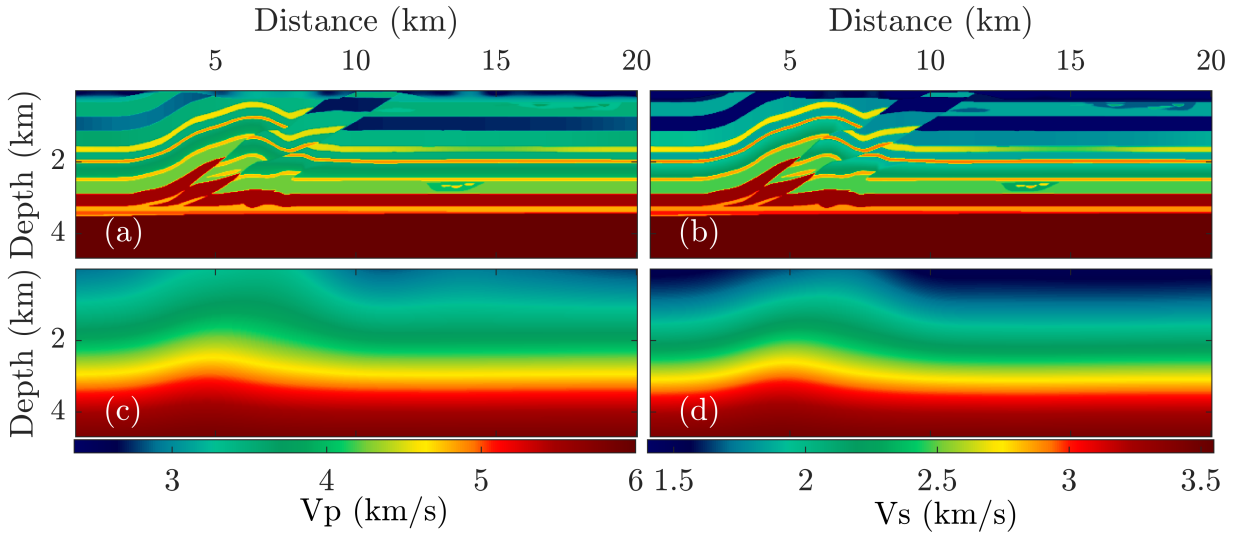


Figure 7: Elastic FWI test. (a-b) True V_p and V_s models, (c-d) initial V_p and V_s models.

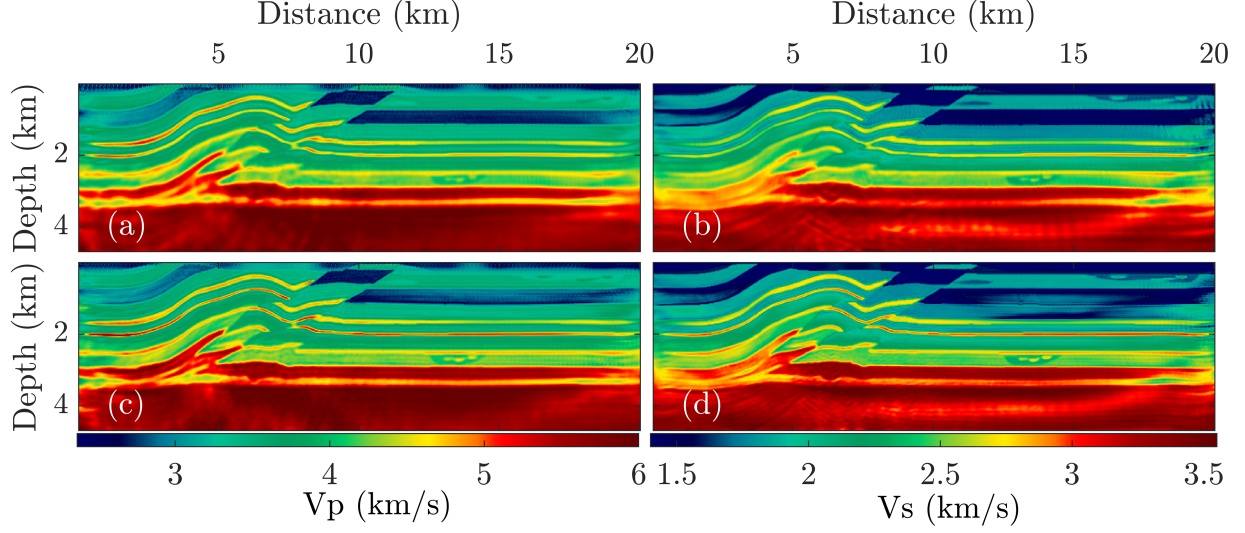


Figure 8: Elastic FWI test. (a-b) Reconstructed V_p and V_s models obtained by the AL method. (c-d) is the same as (a-b) for the case of dual-AL method.

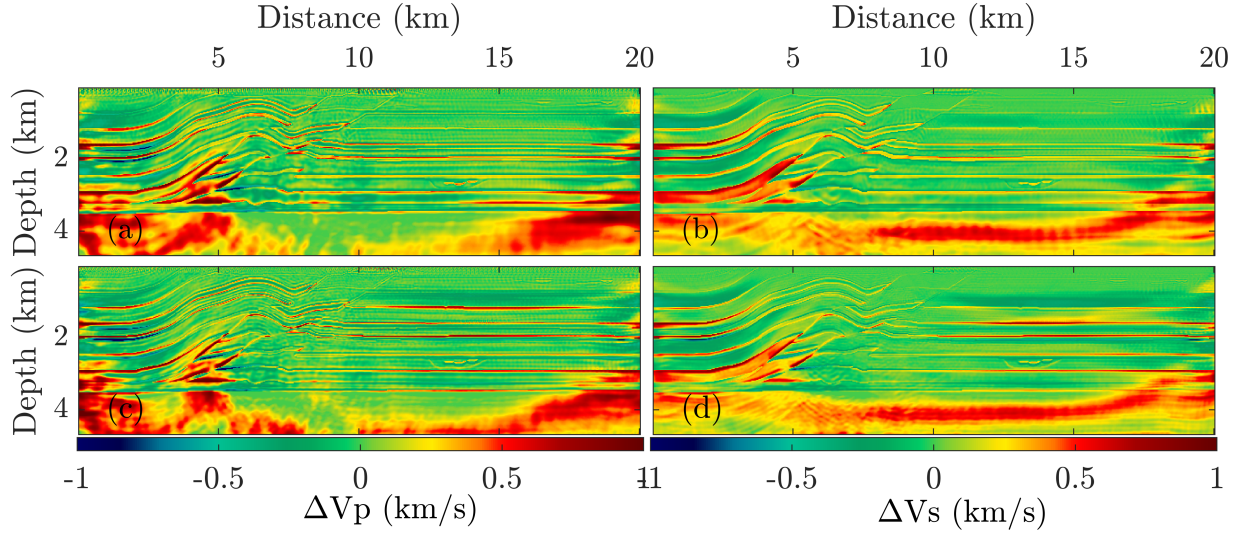


Figure 9: Elastic FWI test. The velocity difference between true models shown in Fig. 7a-b and estimated models shown in Fig. 8. (a-b) V_p and V_s differences for the case of the AL algorithm. (c-d) same as (a-b) for the case of dual-AL algorithm.

6 Discussion

FWI is a nonlinear optimization problem that involves computationally intensive forward calculations, requiring precise discretization of the associated partial differential equations (PDEs) using methods such as finite differences (FD) to generate synthetic data. Traditionally, the problem's nonlinearity is addressed by expanding around an initial model and truncating higher-order terms to produce a linearized problem, which is then solved iteratively to update the model. However, this approach necessitates updating the FD operator and Hessian matrix at each iteration since they depend on the evolving background model.

In this paper, we proposed an alternative FWI algorithm that maintains a fixed background model and focuses on estimating the missing nonlinearity term associated with it. Our approach is based on solving the dual AL functional and provides a standard formulation for keeping the background model fixed while solving FWI.

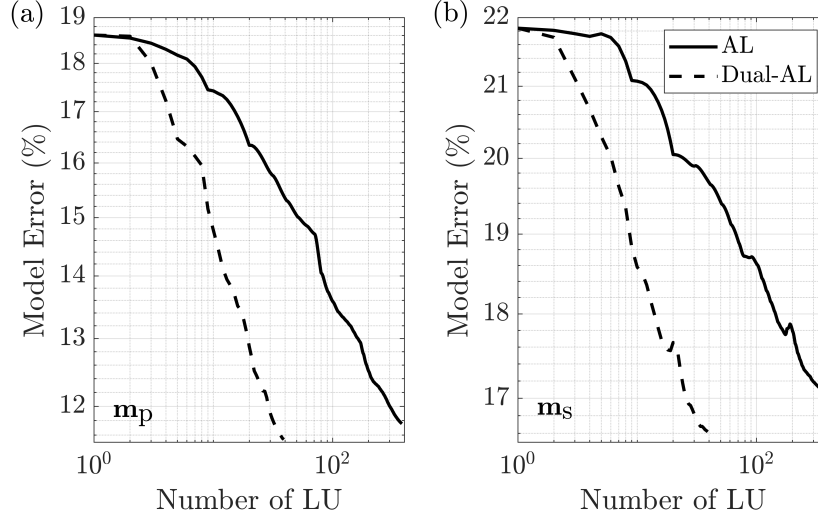


Figure 10: Elastic FWI test. Evolution of the computed model error versus the number of LU factorization for (a) squared V_P model (m_p) and (b) squared V_S model (m_s).

This approach of keeping the background model fixed was first introduced in [34] within the framework of Contrast Source Inversion (CSI). CSI is based on a quadratic penalty formulation, with optimization performed over both the contrast (wavefield) and contrast source (scattering source). This work served as a source of inspiration for the investigations undertaken in [41] and [42]. More specifically, [42] applied this approach to the original wavefield-oriented AL method. However, in their formulation, the computed LU decomposition was used as a preconditioner to solve for the wavefield in an inner loop, requiring additional forward/backward substitutions.

Even though the presented dual algorithm leads to a very significant computational savings, its computational efficiency can be further improved by using source encoding [43] or generalized sketching techniques [30] to limit the number of right-hand sides.

7 Conclusion

We have introduced an efficient algorithm for Full Waveform Inversion (FWI) based on the dual augmented Lagrangian approach. The core innovation of this algorithm lies in its focus on accurately estimating the Lagrange multipliers, which account for the multiple scattering terms inherent to the problem nonlinearity. Once the multipliers are determined, the problem can be effectively linearized and solved with high accuracy for a given background model. This approach allows the finite-difference operator and Hessian matrices to remain fixed throughout the iterations, as they depend solely on the background model. Additionally, the algorithm determines the penalty parameter, its only free parameter, automatically.

Numerical examples using acoustic data demonstrate that the new algorithm can efficiently and automatically reconstruct complex geological models, such as the 2004 BP salt model. The results from elastic data inversion further confirm the algorithm's efficiency and effectiveness in accurately estimating both P-wave and S-wave velocities.

8 Acknowledgments

This research was financially supported by the SONATA BIS grant (No. 2022/46/E/ST10/00266) of the National Science Center in Poland.

References

- [1] J. Virieux and S. Operto, "An overview of full-waveform inversion in exploration geophysics," *Geophysics*, vol. 74, no. 6, pp. WCC1–WCC26, 2009.

- [2] H. S. Aghamiry, A. Gholami, and S. Operto, "Compound regularization of full-waveform inversion for imaging piecewise media," *IEEE Transactions on Geoscience and Remote Sensing*, vol. 58, no. 2, pp. 1192–1204, 2019.
- [3] J. Tromp, "Seismic wavefield imaging of Earth's interior across scales," *Nature Reviews Earth & Environment*, vol. 1, pp. 40–53, 2019.
- [4] D. Feng, S. Ding, X. Wang, and X. Wang, "Wavefield reconstruction inversion of GPR data for permittivity and conductivity models in the frequency domain based on modified total variation regularization," *IEEE Transactions on Geoscience and Remote Sensing*, vol. 60, pp. 1–14, 2021.
- [5] I. Giannakis, A. Giannopoulos, and C. Warren, "Realistic FDTD GPR antenna models optimized using a novel linear/nonlinear full-waveform inversion," *IEEE Transactions on Geoscience and Remote Sensing*, vol. 57, no. 3, pp. 1768–1778, 2018.
- [6] B. Dupuy, A. Romdhane, P. Eliasson, E. Querendez, H. Yan, V. A. Torres, and A. Ghaderi, "Quantitative seismic characterization of CO₂ at the sleipner storage site, north sea," *Interpretation*, vol. 5, no. 4, pp. SS23–SS42, 2017.
- [7] E. Pearce, A. D. Booth, S. Rost, P. Sava, T. Konuk, A. Brisbourne, B. Hubbard, and I. Jones, "Characterising ice slabs in firn using seismic full waveform inversion, a sensitivity study," *Journal of Glaciology*, vol. 69, no. 277, pp. 1419–1433, 2023.
- [8] F. Wittkamp, N. Athanasopoulos, and T. Bohlen, "Individual and joint 2-D elastic full-waveform inversion of Rayleigh and Love waves," *Geophysical Journal International*, vol. 216, no. 1, pp. 350–364, 2018.
- [9] L. Qu, W. Pan, K. Innanen, M. Macquet, and D. Lawton, "Feasibility study of anisotropic full-waveform inversion with DAS data in a vertical seismic profile configuration at the Newell County Facility, Alberta, Canada," *Surveys in Geophysics*, pp. 1–26, 2024.
- [10] S. Klaasen, S. Noe, S. Thrastarson, Y. Cubuk-Sabuncu, K. Jónsdóttir, and A. Fichtner, "Moment tensor inversion with full-waveform inversion and distributed acoustic sensing on a subglacial volcano: Grímsvötn, Iceland," Copernicus Meetings, Tech. Rep., 2024.
- [11] R. G. Pratt, C. Shin, and G. J. Hicks, "Gauss-Newton and full Newton methods in frequency-space seismic waveform inversion," *Geophysical Journal International*, vol. 133, pp. 341–362, 1998.
- [12] Z. Chen, D. Cheng, W. Feng, and T. Wu, "An optimal 9-point finite difference scheme for the Helmholtz equation with PML," *International Journal of Numerical Analysis & Modeling*, vol. 10, no. 2, 2013.
- [13] E. Haber, U. M. Ascher, and D. Oldenburg, "On optimization techniques for solving nonlinear inverse problems," *Inverse problems*, vol. 16, no. 5, p. 1263, 2000.
- [14] J. Nocedal and S. J. Wright, *Numerical Optimization*, 2nd ed. Springer, 2006.
- [15] V. Akçelik, "Multiscale Newton-Krylov methods for inverse acoustic wave propagation," Ph.D. dissertation, Carnegie Mellon University, Pittsburgh, Pennsylvania, 2002.
- [16] H. S. Aghamiry, A. Gholami, and S. Operto, "Improving full-waveform inversion by wavefield reconstruction with the alternating direction method of multipliers," *Geophysics*, vol. 84, no. 1, pp. R139–R162, 2019.
- [17] A. Gholami, H. S. Aghamiry, and S. Operto, "Extended full waveform inversion in the time domain by the augmented Lagrangian method," *Geophysics*, vol. 87, no. 1, pp. R63–R77, 2022.
- [18] S. Operto, A. Gholami, H. Aghamiry, G. Guo, S. Beller, K. Aghazade, F. Mamfoumbi, L. Combe, and A. Ribodetti, "Extending the search space of full-waveform inversion beyond the single-scattering Born approximation: A tutorial review," *Geophysics*, vol. 88, no. 6, pp. R671–R702, 2023.
- [19] G. Golub and V. Pereyra, "Separable nonlinear least squares: the variable projection method and its applications," *Inverse problems*, vol. 19, no. 2, p. R1, 2003.
- [20] T. van Leeuwen and W. A. Mulder, "A correlation-based misfit criterion for wave-equation traveltime tomography," *Geophysical Journal International*, vol. 182, no. 3, pp. 1383–1394, 2010.
- [21] S. Luo and P. Sava, "A deconvolution-based objective function for wave-equation inversion," *SEG Technical Program Expanded Abstracts*, vol. 30, no. 1, pp. 2788–2792, 2011.
- [22] M. Warner and L. Guasch, "Adaptive waveform inversion: Theory," *Geophysics*, vol. 81, no. 6, pp. R429–R445, 2016.
- [23] B. Engquist, B. D. Froese, and Y. Yang, "Optimal transport for seismic full waveform inversion," *Communications in Mathematical Sciences*, vol. 14, no. 8, pp. 2309–2330, 2016.
- [24] W. Ha and C. Shin, "Deconvolution-based objective functions for full waveform inversion in the laplace domain," *IEEE Transactions on Geoscience and Remote Sensing*, vol. 60, pp. 1–8, 2021.

- [25] W. He, G. Hu, and B. Zhang, “Optimal matching full waveform inversion,” *IEEE Transactions on Geoscience and Remote Sensing*, vol. 61, pp. 1–10, 2023.
- [26] T. van Leeuwen and F. J. Herrmann, “Mitigating local minima in full-waveform inversion by expanding the search space,” *Geophysical Journal International*, vol. 195, no. 1, pp. 661–667, 2013.
- [27] T. van Leeuwen and F. J. Herrmann, “A penalty method for PDE-constrained optimization in inverse problems,” *Inverse Problems*, vol. 32, no. 1, p. 015007, 2015.
- [28] A. Gholami and K. Aghazade, “Full waveform inversion and Lagrange multipliers,” *Geophysical Journal International*, p. ggae148, 2024.
- [29] R. T. Rockafellar, “Monotone operators and the proximal point algorithm,” *SIAM journal on control and optimization*, vol. 14, no. 5, pp. 877–898, 1976.
- [30] K. Aghazade, H. S. Aghamiry, A. Gholami, and S. Operto, “Randomized source sketching for full waveform inversion,” *IEEE Transactions on Geoscience and Remote Sensing*, vol. 60, pp. 1–12, 2021.
- [31] D. C. Liu and J. Nocedal, “On the limited memory BFGS method for large scale optimization,” *Mathematical Programming*, vol. 45, pp. 503–528, 1989.
- [32] H. F. Walker and P. Ni, “Anderson acceleration for fixed-point iterations,” *SIAM Journal on Numerical Analysis*, vol. 49, no. 4, pp. 1715–1735, 2011.
- [33] K. Aghazade, A. Gholami, H. Aghamiry, and S. Operto, “Anderson accelerated augmented Lagrangian for extended waveform inversion,” *Geophysics*, vol. 87, pp. R79–R91, 2022.
- [34] A. Abubakar, W. Hu, T. M. Habashy, and P. M. van den Berg, “Application of the finite-difference contrast-source inversion algorithm to seismic full-waveform data,” *Geophysics*, vol. 74, no. 6, pp. WCC47–WCC58, 2009.
- [35] R. A. Tapia, “Diagonalized multiplier methods and quasi-Newton methods for constrained optimization,” *Journal of optimization theory and applications*, vol. 22, pp. 135–194, 1977.
- [36] A. Gholami and S. Gazzola, “Automatic balancing parameter selection for Tikhonov-TV regularization,” *BIT Numerical Mathematics*, vol. 62, no. 4, pp. 1873–1898, 2022.
- [37] H. Sun and L. Demanet, “Extrapolated full-waveform inversion with deep learning,” *Geophysics*, vol. 85, no. 3, pp. R275–R288, 2020.
- [38] K. Aghazade, A. Gholami, H. S. Aghamiry, and H. R. Siahkoohi, “Robust elastic full-waveform inversion using an alternating direction method of multipliers with reconstructed wavefields,” *Geophysics*, vol. 89, no. 3, pp. R287–R302, 2024.
- [39] T. M. Brocher, “Empirical relations between elastic wavespeeds and density in the earth’s crust,” *Bulletin of the seismological Society of America*, vol. 95, no. 6, pp. 2081–2092, 2005.
- [40] J.-B. Chen and J. Cao, “Modeling of frequency-domain elastic-wave equation with an average-derivative optimal method,” *Geophysics*, vol. 81, no. 6, pp. T339–T356, 2016.
- [41] T. Alkhalifah and C. Song, “An efficient wavefield inversion: Using a modified source function in the wave equation,” *Geophysics*, vol. 84, no. 6, pp. R909–R922, 2019.
- [42] H. S. Aghamiry, A. Gholami, and S. Operto, “On efficient frequency-domain full-waveform inversion with extended search space,” *Geophysics*, vol. 86, no. 2, pp. R237–R252, 2021.
- [43] D. Feng, B. Li, X. Wang, D. Xu, C. Cao, T. Yu, Y. Liu, and Z. Feng, “Multiparameter elastic full waveform inversion based on random source-encoding and projection regularization,” *IEEE Transactions on Geoscience and Remote Sensing*, vol. 61, pp. 1–12, 2023.